Eur. Phys. J. B **19**, 9–16 (2001)

THE EUROPEAN PHYSICAL JOURNAL B

EDP Sciences

Phase transitions sequence in pyrochlore $Cd_2Nb_2O_7$ studied by IR reflectivity

E. Buixaderas[1,a], S. Kamba[1], J. Petzelt[1], M. Savinov[1], and N.N. Kolpakova[2]

[1] Institute of Physics, ASCR, Na Slovance 2, 182 21 Prague 8, Czech Republic
[2] A.F. Ioffe Physico-Technical Institute, RAS, Politechnicheskaya 26, 194021 St. Petersburg, Russia

Received 17 July 2000

Abstract. The infrared reflectivity of $Cd_2Nb_2O_7$ single crystal was studied in the temperature interval of 10–540 K, together with complementary dielectric measurements. A ferroelectric soft mode was revealed above the ferroelectric phase transition at $T_c = 196$ K coupled with a central-mode type dispersion in the near-millimetre range. This proves the mixed displacive and order-disorder nature of the transition. Below T_c many new modes were detected due to lowering of the symmetry, especially below the previously suggested incommensurate transition at 85 K. Discussion of the possible phase transitions based on symmetry considerations is presented with the conclusion that the ferroelectric transition is proper with the F_{1u} symmetry of the order parameter, whereas the intermediate ferroelastic transition is improper and triggered by the coupling with the ferroelectric order parameter.

PACS. 78.30-j Infrared and Raman spectra – 63.20-e Phonons in crystal lattices – 77.80.Bh Phase transitions and Curie point

1 Introduction

Crystals having the pyrochlore structure $A_2B_2O_7$, closely related to the perovskite one, are prospective materials which often show ferroelectricity [1]. Detailed investigations are, however, mostly still lacking. One of the most studied representatives of the pyrochlore family is cadmium niobate $Cd_2Nb_2O_7$ (CNO), in which the ferroelectric-ferroelastic state coexists with relaxor, incommensurate and glassy states.

CNO has been reported to undergo seven phase transitions. From the cubic paraelastic-paraelectric $Fd\bar{3}m$-O_h^7 phase it passes through two isostructural phase transitions at $T_i = 512$ K and $T_{tr} = 312$ K [2,3] revealed by a small change in the lattice parameter and in the conductivity. At room temperature, the structure of the crystal can be seen as two interpenetrating networks: a rigid framework of NbO_6 octahedra which share corners and zig-zag Cd-O chains lying along the [110] direction [4,5] (see Fig. 1).

At T_s= 205 K CNO undergoes a ferroelastic transition to an orthorhombic mmm-D_{2h} phase followed by a ferroelectric one with relaxor behaviour ($T_c = 196$ K) [6–8]. Spontaneous polarization was revealed in [110] (Ref. [9]), [111] and [100] directions [7,10] and the new symmetry group was reported as mm2, based on the observation of domain structure changes [11] and refined to Ima2-C_{2v}^{22} from XRD [12].

[a] e-mail: buixader@fzu.cz

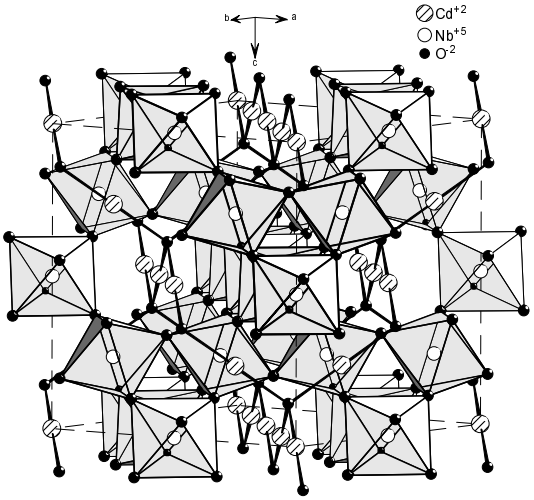

Fig. 1. Structure of CNO at room temperature.

On further cooling, at $T_{inc} = 85$ K, CNO exhibits anomalies in permittivity and in the damping of some new Raman modes [13,14]. This has been interpreted as a feature of incommensurate phase that seems to lock-in at $T_{com} = 46$ K, although the wave-vector of the modulation has not been determined yet. The average symmetry is probably monoclinic [11], the suggested space group I1a1-C_s^4 [15]. Finally a dipolar glassy state is reached below $T_g = 19$ K [16,17].

Dielectric measurements revealed a complex behaviour showing two different relaxational processes

in the permittivity: one in the MHz range, present from T_c to about 150 K, caused by domain wall motion, and another in the kHz range, which dominates below 150 K. The origin of the latter one is not clear. It could be related with some defects, but it was suggested also as caused by reorientation of Cd-O dipole chains [5,18].

Earlier infrared (IR) reflectivity measurements [19] at three temperatures and microwave (MW) data in the ranges of 90–450 K [19] and 120–300 K [20] showed that the ferroelectric transition can be explained by the softening of the lowest IR active mode above T_c. Hardening of two low-frequency Raman modes below T_s and T_c, respectively, was also recently found [8,21].

In this paper we report on thorough measurements of the IR reflectivity over the whole range of phase transitions trying to determine the ferroelectric soft mode behaviour above and below T_c, discuss the dynamic nature of the transition and possibly find support for the incommensurate phase by comparison with the Raman data. Also, we perform the factor group analysis to find the correlation of the polar modes in various phases and suggest order-parameter representations responsible for the equitranslational ferroelastic and ferroelectric phase transitions.

2 Experimental

$Cd_2Nb_2O_7$ single crystal was studied from 540 K down to 10 K by means of far-IR reflectivity and radio-frequency dielectric spectroscopy. The sample was grown by a flux method [4,6]. We used a polished yellow bulk sample (size $8 \times 4 \times 2$ mm^3) for IR reflectivity measurements. A plate of about a 0.25 mm thickness was polished for dielectric measurements.

IR reflectivity measurements were performed with the Fourier spectrometer Bruker IFS 113v equipped with room temperature DTGS pyroelectric detectors as well as He-cooled (1.5 K) Si bolometer. Spectra were measured in the 20–2000 cm^{-1} range (20–650 cm^{-1} below room temperature). For temperature-dependent measurements a continuous-flow Oxford CF 104 cryostat (from 300 to 10 K) and a furnace (300–540 K) were used. Unpolarized light was used because the sample is cubic at room temperature and becomes multidomain at low temperatures.

For dielectric measurements, Au electrodes were evaporated using the BAL-TEX SCD 050 Sputter Coater onto the faces of the plate. An impedance analyser 4192 LF Hewlett-Packard (100 Hz–1 MHz) was used. The sample was heated and cooled in the temperature range of 13–600 K at a velocity rate of 2 K min^{-1} under a measurement field of 40 V cm^{-1}.

3 Results and evaluation

3.1 Far-IR reflectivity measurements

The temperature dependence of the reflectivity of the CNO single crystal is presented in Figure 2. Our room temperature IR reflectivity spectra are in agreement with the previously published ones [19]. We used a resolution of 2 cm^{-1} and therefore we resolved a large number of modes at low temperatures. Experimental spectra were fitted with the generalized oscillator model of the dielectric function due to the presence of broad reflection bands [22]

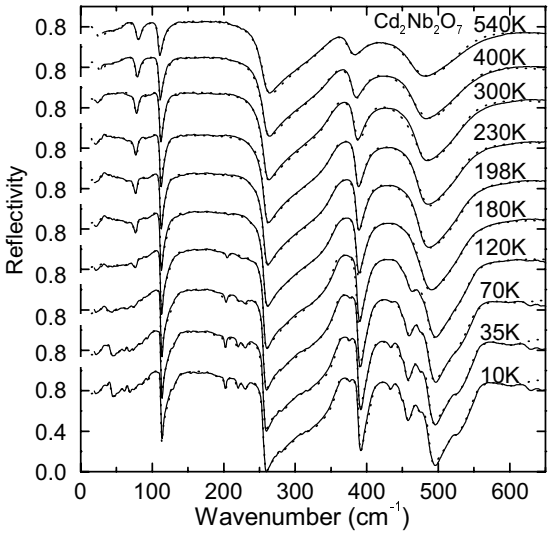

Fig. 2. Temperature dependence of the reflectivity spectra of CNO single crystal. Solid lines correspond to the experiment and dotted lines to the fit.

$$\hat{\varepsilon}(\omega) = \varepsilon'(\omega) + j\varepsilon'' = \varepsilon_\infty \prod_{i=1}^{n} \frac{\omega_{\mathrm{LO}i}^2 - \omega^2 + j\omega\gamma_{\mathrm{LO}i}}{\omega_{\mathrm{TO}i}^2 - \omega^2 + j\omega\gamma_{\mathrm{TO}i}}, \quad (1)$$

where ε_∞ is the permittivity at frequencies much higher than all oscillator eigenfrequencies, $\omega_{\mathrm{TO}i}$ and $\omega_{\mathrm{LO}i}$ are the eigenfrequencies of the transverse and longitudinal ith phonon mode and $\gamma_{\mathrm{TO}i}$ and $\gamma_{\mathrm{LO}i}$ their respective damping constants.

The calculated permittivity is shown in Figure 3. Our dielectric values at 1 MHz and also available microwave data [19,20] were used for fitting the spectra. Calculated loss spectra are depicted in Figure 4 showing the appearance of many new weak modes at low temperatures.

3.2 Dielectric measurements

The results of our dielectric measurements revealed a strong dielectric dispersion below 1 MHz from 190 to 150 K, which show features typical for relaxor ferroelectrics [5,10,18]. This dispersion seems to be caused by the dynamics of polar nanodomains [18,23]. The value of the broad maximum of ε' is higher than previously reported, but sample dependent, giving evidence of the influence of defects and impurities on the dielectric behaviour [21]. It has to be mentioned that the high value of the ac measurements field used can also increase the permittivity peak values.

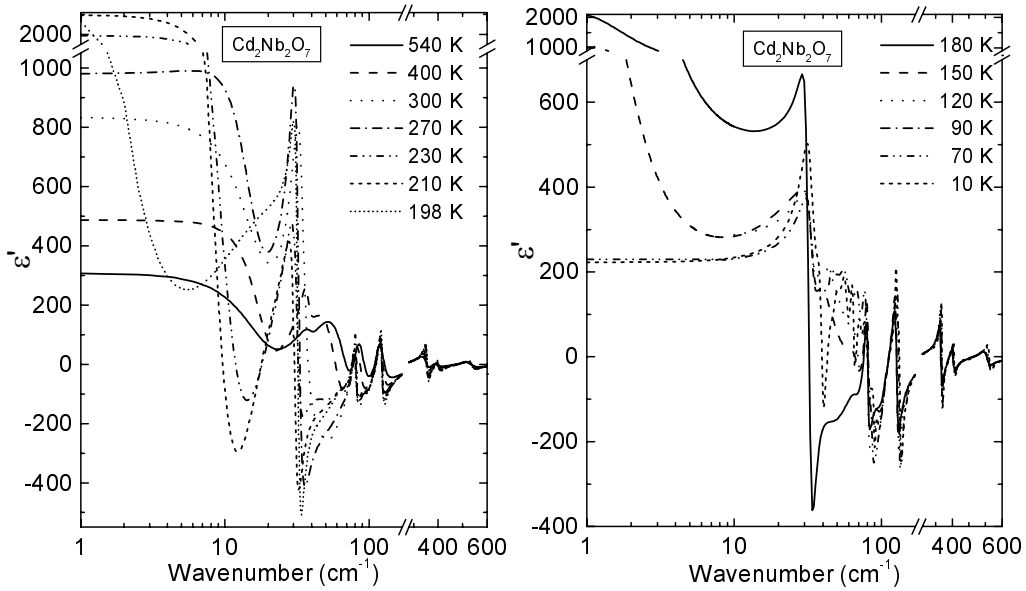

Fig. 3. Temperature dependence of the permittivity obtained from equation (1) for the CNO single crystal. Note the logarithmic scale.

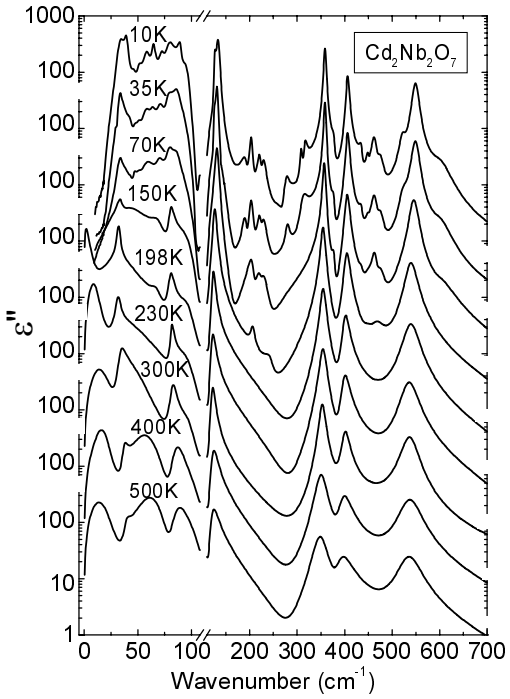

Fig. 4. Temperature dependence of the loss spectra obtained from equation (1) for the CNO single crystal showing the splitting and appearance of new modes. Note the logarithmic scale.

Let us discuss the dielectric dispersion using Figure 5. The figure shows the temperature dependence of the phonon contribution, $\Delta\varepsilon_{\rm ph}$, together with the permittivity at several frequencies measured by us: 1.2 kHz, 14.5 kHz, 100 kHz and 1 MHz (the latter value will be denoted as the quasi-static permittivity ε_0) and also the values at 36 and 78 GHz taken from reference [19].

The quasi-static permittivity ε_0 is much higher than the total contribution from the phonons, $\Delta\varepsilon_{\rm ph}$. This shows by the presence of additional dispersion below the phonon frequencies over the whole temperature range except for the lowest temperatures. A contribution to the permittivity ε' above $T_{\rm c}$ indicates the presence of a central-mode like (CM) dispersion in the MW range. Its contribution is denoted by $\Delta\varepsilon_{\rm CM}$ and the sum of both CM and phonon contributions gives the quasi-static value of the permittivity $\varepsilon_0 = \Delta\varepsilon_{\rm CM} + \Delta\varepsilon_{\rm ph}$ above $T_{\rm c}$. In this range, CM accounts for the most important part of the $\varepsilon'(T)$ anomaly. Below $T_{\rm c}$ the values of ε' at 36 GHz [19] are higher than those at 1 MHz (but this is not the case at 78 GHz [19] and at 4 GHz [20]), which is quite unusual, because it would mean the presence of a resonant mode near this frequency. As such a feature was never observed in other materials in the MW range, we attribute it rather to a difference in samples or measurement error.

3.3 IR modes behaviour

In the high-temperature cubic phase there are 7 IR active modes predicted by factor-group analysis (see below) plus the CM excitation located below the phonon frequencies. We cannot see directly this excitation in our IR spectra because it lies below 20 cm^{-1} but we can infer it from its contribution to the measured MW permittivity [19] and from the minima revealed in the reflectivity spectra around 20 cm^{-1}.

In Figure 6 the temperature evolution of our IR phonon frequencies is presented compared with some of the Raman modes from references [5,14,21]. It can be seen that the mode located at 70 cm^{-1} softens down to 40 cm^{-1} towards $T_{\rm c}$, as well as the CM which softens from 22 cm^{-1} to the GHz range, leaving in between an intermediate weakly temperature dependent mode. The softening

$$\hat{\varepsilon}(\omega) = \frac{\Delta\varepsilon_1\omega_1^2(\omega_2^2 - \omega^2 + j\omega\gamma_2) + \Delta\varepsilon_2\omega_2^2(\omega_1^2 - \omega^2 + j\omega\gamma_1) - 2\sqrt{\Delta\varepsilon_1\Delta\varepsilon_2}\omega_1\omega_2\alpha}{(\omega_1^2 - \omega^2 + j\omega\gamma_1)(\omega_2^2 - \omega^2 + j\omega\gamma_2) - \alpha^2} + \sum_{i=3}^{n} \frac{\Delta\varepsilon_i\omega_i^2}{(\omega_i^2 - \omega^2 + j\omega\gamma_i)} + \varepsilon_\infty. \quad (2)$$

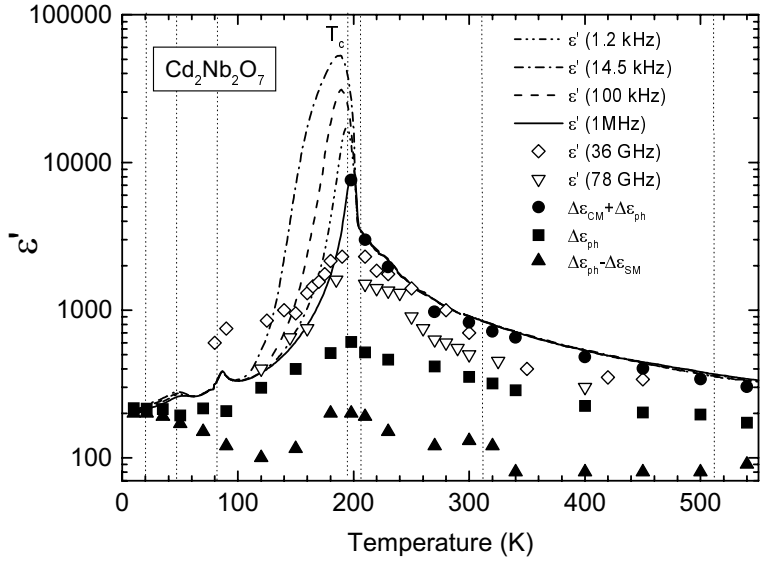

Fig. 5. Temperature dependence of the permittivity showing values measured at several frequencies, the central mode and the phonon contributions. (MW values at 36 and 78 GHz from [19]).

of the CM was already observed in the MW range above T_c [20] and was interpreted as the driving soft mode (SM) of the ferroelectric transition. However, from our data we see that the phonon SM also exists at much higher frequencies, in agreement with the earlier IR measurements [19], and the coupling between these two excitations leads to the softening of the CM (see below).

The occurrence of the two isostructural transitions at 512 and 312 K is not revealed by any important features in the spectra. Splitting of the SM and the mode near 80 cm^{-1} occurs on approaching the ferroelastic phase transition at T_s = 205 K. From the structural point of view, the most important change in CNO in this range is the change in the mean position of Cd atoms which shift from a general Wyckoff position at high temperatures to the (000) position at room temperature [24]. X-ray diffraction data [24] also show dynamic disorder of Cd atoms which are located off-centre, randomly distributed at 0.1 Å from the central position. This is in agreement with the presence of the CM above T_c, which can be assigned to the Cd-hopping among the possible positions. According to references [5,8,21,24], the octahedra framework deforms with the temperature and this influences the Cd-O, which adjust to the change. The Nb atoms do not show disorder, therefore the SM can be assigned to the NbO_6 octahedra stretching coupled with the quasi-harmonic vibrations of Cd.

The above idea can be supported by a two-coupled-oscillators model used to fit the spectra. In this case the dielectric function can be treated as a sum of n damped oscillators, two of them being coupled by a real coupling constant α which renormalizes their frequencies [25]

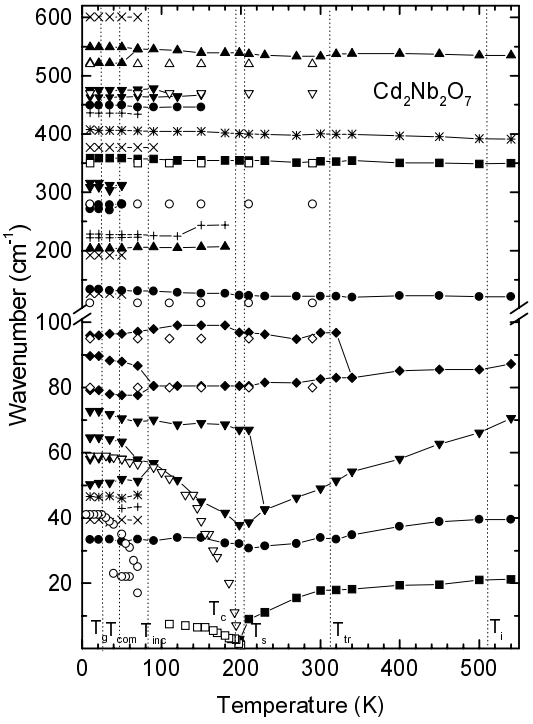

Fig. 6. Temperature dependence of the IR modes frequencies of CNO single crystal obtained from our fit. Open symbols denote Raman modes from [5,14,21].

See equation (2) above.

We coupled the CM and SM leaving uncoupled the weak intermediate mode below 40 cm^{-1}. We were able

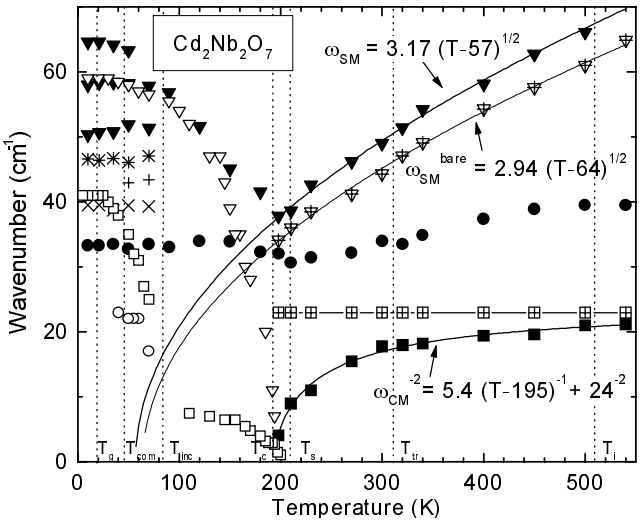

Fig. 7. Temperature dependence of the mode frequencies below 70 cm^{-1}. Bare SM and CM (modes ω_1, ω_2 from Eq. (2)) are marked by crossed open symbols. Full lines denote fits with Cochran law. Full symbols – SM and CM from equation (1). Open symbols – Raman modes [14,21].

to reproduce the spectra as well as the behaviour of the permittivity at 1 MHz using temperature-independent bare CM parameters and coupling constant (ω_{CM} = 23 cm^{-1}, $\Delta\varepsilon_{CM} = 53$, $\gamma_{CM} = 30$ cm^{-1}, $\alpha = -730$ cm^{-2}), just changing the frequency and damping of the SM (but maintaining its oscillator strength, $f_{SM} = \Delta\varepsilon_{SM}\omega_{SM}^2$, constant). The bare and coupled frequencies together with the other observed modes in the low-frequency range are shown in Figure 7. The intermediate mode seems to be temperature-independent down to 300 K and then it becomes also weakly coupled with the other two modes. This is the reason for a slight enhancement of the coupling constant (to −770) below 270 K in our two-coupled-oscillators model. In both models (factorized permittivity – Eq. (1) and coupled modes – Eq. (2)), the optical soft mode follows the Cochran law $\omega = A(T - T_c)^{1/2}$, with very similar parameters (Fig. 7). The critical softening temperature lies near 60 K, which means that the coupling with CM triggers the ferroelectric transition at the much higher temperature of 195 K.

Analysis of the softening of the mode near 60 cm^{-1} was also done on a ceramic sample by Poplavko *et al.* [19] with the critical T_c around 175 K. They were not able to resolve the two soft excitations because they did not assume the existence of the CM. Therefore they assigned the dielectric strength $\Delta\varepsilon_{CM}$ of the CM to the SM. Also, they fail to explain the observed decrease in the reflectivity at 55 cm^{-1} on cooling from 300 to 90 K. In our spectra it is seen that the minimum appears in this region as a result of the SM softening to frequencies lower that 55 cm^{-1} and due to the decrease in its damping.

Below T_c the central component was removed from our fits because its contribution is masked by the contribution to the permittivity of domain wall motion, although it seems to persist weakly in the GHz range [20] as can be seen from Figure. 5. We can identify also the hardening of the SM below T_c, which coincides with the published Raman data [14,21]. Its oscillator strength f_{SM} is shared with the new modes appearing on lowering the temperature. Other good coincidences between Raman and IR mode frequencies are shown in Figures 6 and 7.

On further cooling below T_c several new modes were observed in reflectivity (Fig. 2) and dielectric loss spectra (Fig. 4). From the analysis of the mode parameters, comparing the dielectric and oscillator strength of the new modes, it was possible to distinguish the splitting of degenerate modes from the activation of new ones. In Table 1 the evolution of the transverse mode parameters is presented at several relevant temperatures. The three F_{1u} triplets near 70, 80 and 550 cm^{-1} completely split at low temperature. Some new modes appearing below T_c ($\omega \sim 200$, 220, 450 cm^{-1}) split into two components.

Below T_{inc} many new modes appear. This can be taken as a support for symmetry lowering from orthorhombic to monoclinic symmetry. However we do not see additional softening of any phonon, unlike the Raman spectra [13,14] for which anomalous changes in frequency, damping and strengths were reported. The analysis of the new mode dampings does not reveal anomalies that would enable us to support the conclusion about the incommensurate modulation. It has to be mentioned that the new modes detected are very weak and it is possible that some of them are overlapping so that we could not distinguish them in the spectra. Our conclusion about the absence of incommensurate modulation is therefore not strict.

4 Discussion

So far no attempt was undertaken to formulate the Landau theory for the phase-transition sequence in CNO. The presence of two close phase transitions at 205 and 196 K of different nature makes the determination of the order parameters difficult. From domain observation [11], EPR [8] and Raman [21] experiments these two transitions are, however, clearly distinguished, the point groups of the distorted phases being mmm and mm2, respectively.

From the symmetry point of view we can imagine three possibilities for these phase transitions to occur homogeneously in the whole crystal: (a) consecutively (step by step) by two order parameters transforming according to irreducible representations of the cubic (describing the ferroelastic transition) and orthorhombic phase (describing the ferroelastic-ferroelectric transition); (b) by two coupled order parameters transforming according to two irreducible representations of the cubic group and (c) by two order parameters where the one describing the ferroelectric transition transforms as a reducible representation of the cubic group, (see Tab. 2).

In the case (a), E_g or F_{2g} irreducible representations of the group m3m could be responsible for a proper ferroelastic transition, both leading to mmm symmetry and 6 ferroelastic domains [26]. Then, one of the B_{1u}, B_{2u} or B_{3u} representations of the ferroelastic phase could be responsible for the proper ferroelectric transition resulting in mm2,

Table 1. Parameters of the IR active modes (frequency ω_T and damping γ_T in cm^{-1}) at different temperatures. Asterisk denote activation of new modes.

540 K			198 K			90 K			10 K		
ω_T	γ_T	$\Delta\varepsilon$	ω_T	γ_T	$\Delta\varepsilon$	ω_T	γ_T	$\Delta\varepsilon$	ω_T	γ_T	$\Delta\varepsilon$
21	28	130	2.5	10	6980	-			-		
39	8.5	10	32	3.6	155	33	5.1	33	33	7.2	79
-			-			-			*40	3.4	19
-			-			-			*47	4.5	3.1
-			-			-			51	6.7	9.5
71	35	82	38	43	401	57	22.2	95	58	6.2	19
-			-			-			65	3.2	9.8
-			67	11	7.9	70	7.7	13	73	5.4	8.7
87	21.4	49	80	5.8	16	80	9.6	30	79	9.9	30
-			-			-			90	3.4	0.02
-			97	14	4.6	98	26.2	5.5	96	9.0	11
-			-			-			*127	3.2	2.2
121	20.6	22	123	7.3	16	131	6.9	21	134	7.0	18
-			-			-			*193	13.3	0.13
-			-			*206	14.5	0.25	204	6.6	0.21
-			-			-			222	9.0	0.13
-			-			*225	25.6	0.23	229	12.0	0.12
-			-			-			*272	6.7	0.001
-			-			-			*278	3.6	0.01
-			-			-			*309	5.3	0.06
-			-			-			*316	7.1	0.06
350	34.5	4.2	355	12	4.5	357	6.2	4.1	359	5.1	3.5
-			-			*377	9.4	0.08	377	7.7	0.06
391	41.5	1.6	401	15	1.6	404	11.3	1.7	408	7.1	1.5
-			-			-			*436	7.4	0.03
-			-			*446	19.2	0.01	450	4.7	0.006
-			-			*463	14.2	0.09	463	11.9	0.16
-			-			*478	26.8	0.06	475	15.7	0.07
-			-			-			522	11.5	0.09
535	55.5	1.8	539	33	1.8	545	19.4	1.7	549	13.9	1.6
-			-			-			*601	50.0	0.14

m2m or 2mm symmetry, respectively, spontaneous polarization P_s along one of the cubic axis and 12 ferroelectric domains. The [100] direction of the ferroelastic domain walls was found experimentally [11]. Using published tables [26,27], it can be found that these domain walls are allowed (together with the [110] type of walls) only if the spontaneous strain tensor has the form induced by the F_{2g} representation. However, if the ferroelastic transition is improper, as suggested by the absence of soft Raman mode above T_s, multiplication of the unit cell is required and structural data are needed before drawing any conclusion about the order parameter symmetry. In this case the ferroelectric transition should at least preserve the larger unit cell and the transition should be treated as improper ferroelectric with respect to the cubic phase. This however contradicts the strong dielectric anomaly and the appearance of the SM and CM in the cubic phase.

In case (b) the direct transition from the cubic to ferroelectric phase can be achieved by the order parameter transforming as F_{1u} or F_{2u} representations of the m3m group leading to 2mm symmetry, but with the polarization along the [110] diagonal, and 12 ferroelectric domains, 6 of which are ferroelastic. This case is compatible with the measurements of P_s [9] and with the coexistence of two types of domains [21]. This is also the case when an electric field is applied and suppresses the ferroelastic phase [11]. Out of the two representations just one, F_{1u}, results in a proper ferroelectric phase, which is expected taking into account the IR activity of the SM above T_c. This order parameter should be coupled with the one which leads to the triggered intermediate ferroelastic phase (either proper or improper).

In case (c) two reducible representations $E_g + F_{1u}$ or $F_{2g} + F_{1u}$ for the order parameter symmetry of the ferroelectric transition are possible, leading to the mm2 symmetry, 6 ferroelastic and 6 ferroelectric domains and $P_\mathrm{s} \parallel c$ [26]. However, this possibility is against the spirit of the Landau theory which requires an order parameter transforming according to an irreducible representation. Moreover, this case would require a E_g or F_{2g} Raman active SM which contradicts the experiments.

The absence of the ferroelastic SM and acoustic softening above T_s excludes the proper ferroelastic case, but the presence of the ferroelectric SM in the cubic phase requires a proper ferroelectric transition (without multiplication of the unit cell). Therefore we can conclude that the only possibility is case (b) with the F_{1u} ferroelectric order parameter coupled with another order parameter outside the Brillouin zone centre which triggers the intermediate improper ferroelastic phase (with unit cell multiplication).

Table 2. Factor group analysis of $Cd_2Nb_2O_7$ showing the possible equitranslational ferroelastic and ferroelectric phase transitions at T_s and T_c. The correlation between the irreducible representations is shown in square brackets.

Cubic m3m-O_h Paraelectric phase	Orthorhombic mmm-D_{2h} Ferroelastic phase	Orthorhombic mm2- C_{2v} Ferroelectric phase		
m3m 8 F_{1u} (x,y,z) 4 F_{2g} (xy,xz,yz) 4 F_{2u} (-) 2 F_{1g} (-) 3 E_u (-) E_g (xx,yy,zz) A_{1g} (xx,yy,zz) 3 A_{2u} (-)	$F_{2g} - \boxed{m_{xy}m_{\bar{x}y}m_z}$ 6 domains [100] $u = \begin{pmatrix} a & & \\ & a & d \\ & & -2a \end{pmatrix}$ DW 100, 110 14 $B_{1u}(z)$ [F_{1u}+E_u+A_{2u}] 12 $B_{2u}(y)$ [F_{1u}+F_{2u}] 12 $B_{3u}(x)$ [F_{1u}+F_{2u}] 3 $B_{1g}(xy)$ [E_g+F_{1g}] 6 $B_{2g}(xz)$ [F_{2g}+F_{1g}] 6 $B_{3g}(yz)$ [F_{2g}+F_{1g}] 6 $A_g(xx,yy,zz)$ [F_{2g}+E_g+A_{1g}] 7 A_u (-) [F_{2u}+E_u]	$B_{1u} - \boxed{m_{xz}m_{yz}2_z}$ P_s|| (001) 6x2=12 domains 20 A_1 [A_g+B_{1u}] 18 B_1 [B_{2g}+B_{3u}] 18 B_2 [B_{2u}+B_{3g}] 10 A_2 [A_u+B_{1g}]	$B_{2u} - \boxed{m_{xy}2_ym_{yz}}$ P_s|| (010) 6x2=12 domains 18 A_1 [A_g+B_{2u}] 20 B_1 [B_{1u}+B_{3g}] 15 B_2 [B_{1g}+B_{3u}] 13 A_2 [A_u+B_{2g}]	$B_{3u} - \boxed{2_xm_{xy}m_{xz}}$ P_s|| (100) 6x2=12 domains 18 A_1 [A_g+B_{3u}] 15 B_1 [B_{1g}+B_{2u}] 20 B_2 [B_{1u}+B_{2u}] 13 A_2 [A_u+B_{3g}]
Direct ferroelectric	$F_{1u} - \boxed{2_{xy}m_{xy}m_z}$ Proper ferroelectric P_s|| (110) 12 (6) domains 18 A_1 [A_{1g}+E_g+F_{1u}+F_{2g}+F_{2u}] 15 B_1 [A_{2g}+E_g+F_{1g}+F_{1u}+F_{2u}] 20 B_2 [A_{2u}+E_u+F_{1g}+F_{1u}+F_{2g}] 13 A_2 [A_{1u}+E_u+F_{1g}+F_{2g}+F_2]		$F_{2u} - \boxed{2_{xy}m_{xy}m_z}$ Improper ferroelectric P_s|| (110) 12 (6) domains 18 A_1 15 B_1 20 B_2 13 A_2	
Reducible rep.	F_{2g} +F_{1u} – $\boxed{m_xm_y2_z}$ P_s|| (001) 6 ferroelastic + 6 ferroelectric domains		E_g +F_{1u} – $\boxed{m_xm_y2_z}$ P_s|| (001) 6 ferroelastic + 6 ferroelectric domains	

We performed also the factor-group analysis [28] in the cubic phase using published site symmetry of the atoms [24]. The following modes in the centre of the Brillouin zone are predicted: $8F_{1u}$(IR, acoust.) + $4F_{2u}(-)$ + $2F_{1g}(-)$ + $4F_{2g}$(R) + $3E_u(-)$ + E_g(R) + A_{1g}(R) + $3A_{2u}(-)$. Note that one F_1u triplet stands for the three acoustic modes. In total there are 66 modes (63 optic), which follows from two formula units in the primitive unit cell, $Z = 2$. Out of them, 7 F_{1u} modes are IR active. This result differs from that in reference [19], where 8 IR active modes were predicted although the total number of modes was the same.

In the ferroelastic mmm-D_{2h} phase, a splitting is expected for the F_{1u} IR and F_{2g} Raman triplets and E_g doublet as well as activation of the silent F_{2u} and F_{1g} modes. This results in 38 IR active modes out of the 66 ones (without taking into account the possible multiplication of the unit cell) (see Tab. 2). In the ferroelectric phase the reported loss of centre of symmetry [29] requires activation of all the optic modes, out of which the A_1, B_1 and B_2 ones become simultaneously IR and Raman active and A_2 ones just Raman active.

5 Conclusions

Far IR reflectivity measurements in CNO showed that the dynamic origin of the ferroelectric transition from the paraelectric cubic phase consists in a polar SM coupled with an overdamped excitation in the near-millimetre range, which is probably caused by the dynamic disorder of Cd atoms. The nature of the ferroelectric phase transition is therefore of the mixed displacive and order-disorder type. From the symmetry point of view the transition is proper ferroelectric and the order parameter transforms according to the F_{1u} representation of the cubic m3m point group. On the other hand, the intermediate ferroelastic phase seems to be improper. Structural data are needed for the determination of the multiplication of the unit cell in the ferroelastic phase and to support the hypothesis of the incommensurate phase.

The work was supported by the Grant Agency of the Czech Rep. (project No. 202/98/1282), Grant Agency of the Acad. Sci. Oh the Czech Rep. (project No A1010828) and the Basque Government (Ph.D scholarship of the program "Formación de investigadores del Dep. de Educación, Universidades e Investigación").

References

1. V.A. Isupov, Ferrolectrics Rev. **2**, 115 (2000).
2. N.N. Kolpakova, R. Margraf, A. Pietraszko, Fiz. Tvrd. Tela **29**, 3629 (1987).
3. N.N. Kolpakova, A. Pietraszko, S. Waplak, L. Szczepanska, Sol. State Comm. **79**, 707 (1991).
4. F. Jona, G. Shirane, R. Pepinsky, Phys. Rev. **98**, 903 (1955).

5. N.N. Kolpakova, M. Wiesner, G. Kugel, P. Bouson, Ferroelectrics **190**, 179 (1997).
6. G.I. Golovshchikova, V.A. Isupov, I.E. Myl'nikova Fiz. Tverd. Tela **13**, 2349 (1971).
7. N.N. Kolpakova, R. Margraf, A. Petrasko, Fiz. Tvrd. Tela **29**, 2638 (1987).
8. N.N. Kolpakova, S. Waplak, W. Bednarski, J. Phys. Cond. Matt. **10**, 9309 (1998).
9. G.A. Smolenski, N.N. Krainik, L.S.Kamzina, F.M. Salaev, E.A. Tarankov, E.S. Sher, Jpn J. App. Phys. **24**, Supl. 24-2, 820 (1985).
10. V.A. Isupov, G.N. Tarasova, Fiz. Tverd. Tela **25**, 1018 (1983).
11. Z.G. Ye, N.N. Kolpakova, J.P. Rivera, H. Schmid, Ferroelectrics **124**, 275 (1991).
12. A. Kuster, J. Ihringer, W. Prandl, H. Ritter, Acta Cryst. A **46**, C-262 (1990).
13. G.A. Smolenski, N.N. Kolpakova, S.A. Kizhaev, E.S. Sher, Ferroelectrics **73**, 161 (1987).
14. N.N. Kolpakova, G. A. Smolensky, I.G. Siny, E.G. Kuzminov, S.D. Prokhorova, V.D. Mikvabia, I.E. Mylnikova, J. Phys. Soc. Jpn **49**, Supl. b, 32 (1980).
15. A. Küster, Ph.D. thesis, University of Tübingen, 1992.
16. W.N. Lawless, Ferroelectrics **37**, 627 (1981).
17. N.N. Kolpakova, B. Hilczer, M. Wiesner, Phase Transitions **47**, 113 (1994).
18. N.N. Kolpakova, I.L. Shulpina, M.P Shcheglov, S. Waplak, W. Bednarski, W. Nawrocik, M. Wiesner, Ferroelectrics **240**, 265 (2000), N.N. Kolpakova, N.N. Kolpakova, M. Wiesner, G. Kugel, P. Bourson, Ferroelectrics **201**, 107 (1997).
19. Y.M. Poplavko, A. S. Kiyasev, V.O. Sarakhov, V.G. Tsikaloc, V.V. Aleksejev, Fiz. Tvrd. Tela **16**, 713 (1974).
20. J. Banys, J. Grigas, N.N. Kolpakova, R. Sobiestijankas, E. Sher, Liet. Fiz. Rinkinys **29**, 209 (1989).
21. N.N. Kolpakova, M. Wiesner, I.L. Shul'pina, P.P.Syrnikov, Ferroelectrics **221**, 91 (1999).
22. F. Gervais, *Infrared and Millimeter waves*, Vol. 8, Chap. 7, edited by K.J. Button, (Ac. Press, New York, 1983), p. 279.
23. C. Ang, R. Guo, A.S. Bhalla, E.L. Cross, J. Appl. Phys. **87**, 7452 (2000).
24. K. Lukaszewicz, A. Pietraszko, J. Stepién-Damm, Mat. Res. Bull. **29**, 987 (1994).
25. J. Petzelt, G.V. Kozlov, V.V. Volkov, Ferroelectrics **73**, 101 (1987).
26. V. Janovec, V. Dvorak, J. Petzelt, Czech J. Phys B **25**, 1362 (1975).
27. J. Sapriel, Phys. Rev. B **12**, 5128 (1975).
28. D.L. Rousseau. R.P. Baumann, S.P.S. Porto, J. Raman Spectr. **10**, 253 (1981).
29. N.N. Kolpakova, E.S. Sher, S. Waplak, Ferroelectrics **111**, 257 (1990).